OPEN ACCESS

University of BRISTOL

Link to publication record in Explore Bristol Research
PDF-document

On the origins of the compressive cochlear nonlinearity

Robert Szalai,[a)] Alan Champneys, and Martin Homer[b)]

Department of Engineering Mathematics,

University of Bristol,

UK

Dáibhid Ó Maoiléidigh

Max Planck Institute for the Physics of Complex Systems,

Dresden,

Germany.

Current Address: Howard Hughes Medical Institute and Laboratory of Sensory

Neuroscience,

The Rockefeller University,

New York,

USA

Helen Kennedy

Department of Physiology and Pharmacology,

University of Bristol,

UK

Nigel Cooper

School of Life Sciences,

Keele University,

UK

(Dated: July 1, 2011)

Abstract

Various simple mathematical models of the dynamics of the organ of Corti in the mammalian cochlea are analysed. The models are assessed against their ability to explain the compressive nonlinear response of the basilar membrane. The specific models considered are: phenomenological Hopf and cusp normal forms, a recently-proposed description combining active hair-bundle motility and somatic motility, a reduction thereof, and finally a new model highlighting the importance of the coupling between the nonlinear transduction current and somatic motility. The overall conclusion is that neither a Hopf bifurcation nor cusp bifurcation are necessary for realistic compressive nonlinearity. Moreover, two physiological models are discussed showing compressive nonlinearities similar to experimental observations without the need for tuning near any bifurcation.

I. INTRODUCTION

In this paper we will examine different simple local nonlinear mathematical models of the organ of Corti in the mammalian inner ear (illustrated schematically in Fig. 1), comparing and contrasting their strengths and weaknesses. The main test we shall apply to the models is their ability to capture experimentally observed features of the dynamics in response to a pure tone input of varying intensity. In particular, we are interested in the four key aspects of the active hearing process proposed by Hudspeth[1]: significant *amplification* at low sound pressure levels (SPL) (down to 0 dB), *sharp tuning* through a place theory of hearing where different positions along the cochlea respond to different frequencies, *compressive nonlinearity* to reduce 6 magnitudes of SPL variation into 3 magnitudes of basilar membrane vibration; and spontaneous *otoacoustic emissions* whereby most ears continuously output
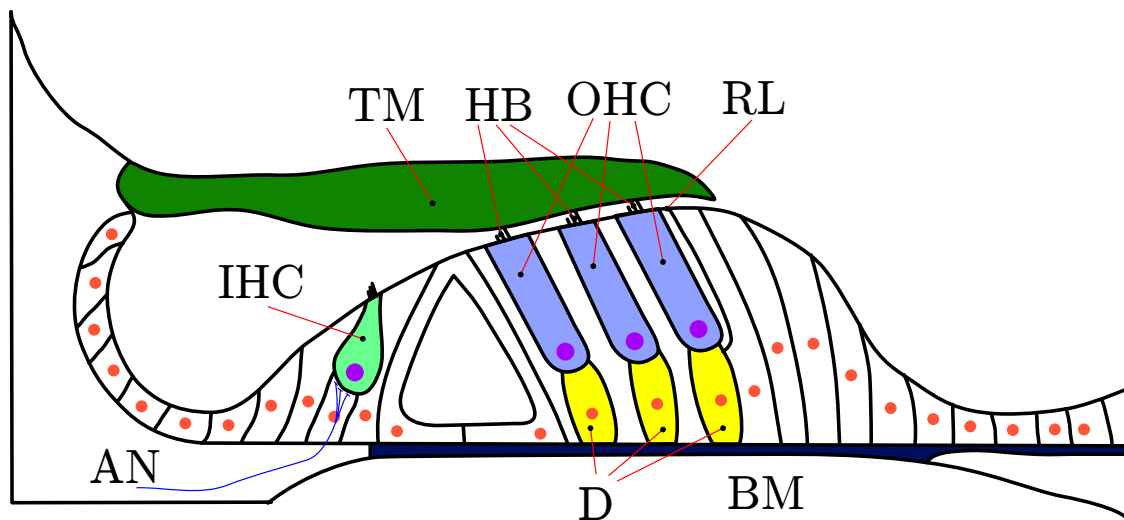
FIG. 1. (color online) Schematic diagram of a cross-section through the organ of Corti of the mammalian cochlea, showing the locations of the basilar membrane (BM), Deiters' cells (D), outer hair cells (OHC), the reticular lamina (RL), hair bundles (HB), tectorial membrane (TM), inner hair cells (IHC) and one auditory nerve (AN) fiber.

---

[a])Electronic address: `r.szalai@bristol.ac.uk`

[b])Electronic address: `martin.homer@bristol.ac.uk`

3

low levels of sound at one or more frequencies.

It is widely held that the active process originates in the outer hair cells (OHC), via transduction channels in their hair bundles that allow a current to pass, which changes the somatic membrane potential. This modulation of membrane potential leads, through the OHC's somatic motility, to significant changes in the configuration of the organ of Corti. The motion of the OHC may lead to mechanical amplification of the organ of Corti's motion. On the other hand, the active motility of the hair bundles has also been proposed as a mechanism for mechanical amplification. There is currently debate about which type of motility is the primary mechanism for amplification. There is some hope that local models might be able to resolve this debate, and this leads to our interest to examine such models using the tools of nonlinear dynamical systems.

The rest of this paper is outlined as follows. We begin, in Sec. II by describing in detail experimental evidence on the function of mammalian OHCs. This includes direct BM displacement measurement obtained by Rhode[2], who examined the chinchilla cochlea in detail, and the results of Kennedy *et al.*[3] who measured the response of OHC hair bundles to mechanical stimulation. The following four sections then discuss a range of models that aim to explain this observed behavior. Sections III and IV discuss and analyse two phenomenological models: one the normal form of a Hopf oscillator, the other the (simpler) normal form of a cusp bifurcation. In particular, we show that the cusp model obeys the same 1/3-power compressive nonlinearity as the Hopf oscillator, at least for sufficiently high input amplitude. Furthermore, we show that the cusp model can show tuning, as the Hopf model does if it is coupled to a simple linear equation for the BM.

The next three sections consider two physiologically-inspired models. Sec. V examines a model introduced by Ó Maoiléidigh and Jülicher[4] that includes the effects of myosin motor adaptation of hair bundles in addition to somatic motility. This model is shown to produce a flatter than 1/3-power response curve at the CF, as seen in Rhode's data. A bifurcation analysis reveals that while the unforced version of this model can produce Hopf bifurcations (and indeed cusps) neither is key to the observed forced response. Section VI introduces

a modification of the Ó Maoiléidigh and Jülicher model, which only includes transduction current nonlinearity, but not active hair bundle motility and a novel hypothesis for the coupling through somatic motility back to the BM position and velocity. This model is also able to provide a qualitative match to the experimental data, while having a minimal number of tunable parameters which are physiologically measurable. We also note that this model can accomodate a Hopf bifurcation, even though it does not include hair bundle motility. Finally, Sec. VII draws conclusions and suggests avenues for future research.

II. REVIEW OF EXPERIMENTAL EVIDENCE

A typical basilar membrane response, taken from the work of Rhode[2], is shown in Fig. 2. There are several important features to notice from the data. From Fig. 2(a) we see that the response is the highest at CF for input below 60 dB, it is nearly linear below CF and the nonlinearity does not vanish with higher forcing frequencies; only the amplitude diminishes. The nature of the nonlinear compression is also interesting. Previously, based on early experimental data[5], it has been argued that the active process provides a compressive nonlinearity with a universal 1/3-power law (see Ref. 1 and references therein). That is, the growth of amplitude at the CF should be uniformly 1/3 for a wide range of input amplitudes (although linear for very small and very large sound inputs). However, more recent data[2] indicates that the compression can be much flatter than 1/3. The data are even consistent with the possibility of saturation (a zero rate of growth) for certain input levels, that is, where the BM amplitude would not vary with small variations of the stimulation level.

Figure 3 presents data from Kennedy *et al.*[3] on the nonlinear response of individual OHC hair bundles of rats. These data were obtained by direct mechanical stimulation of the hair bundles, from organ of Corti preparations with the tectorial membrane surgically removed. Again, several interesting aspects emerge from these data. Note, for example from panel (d), how the bundle exhibits a negative stiffness for moderate sized displacement provided the stimulation has been applied for more than about 3ms. For both small or large
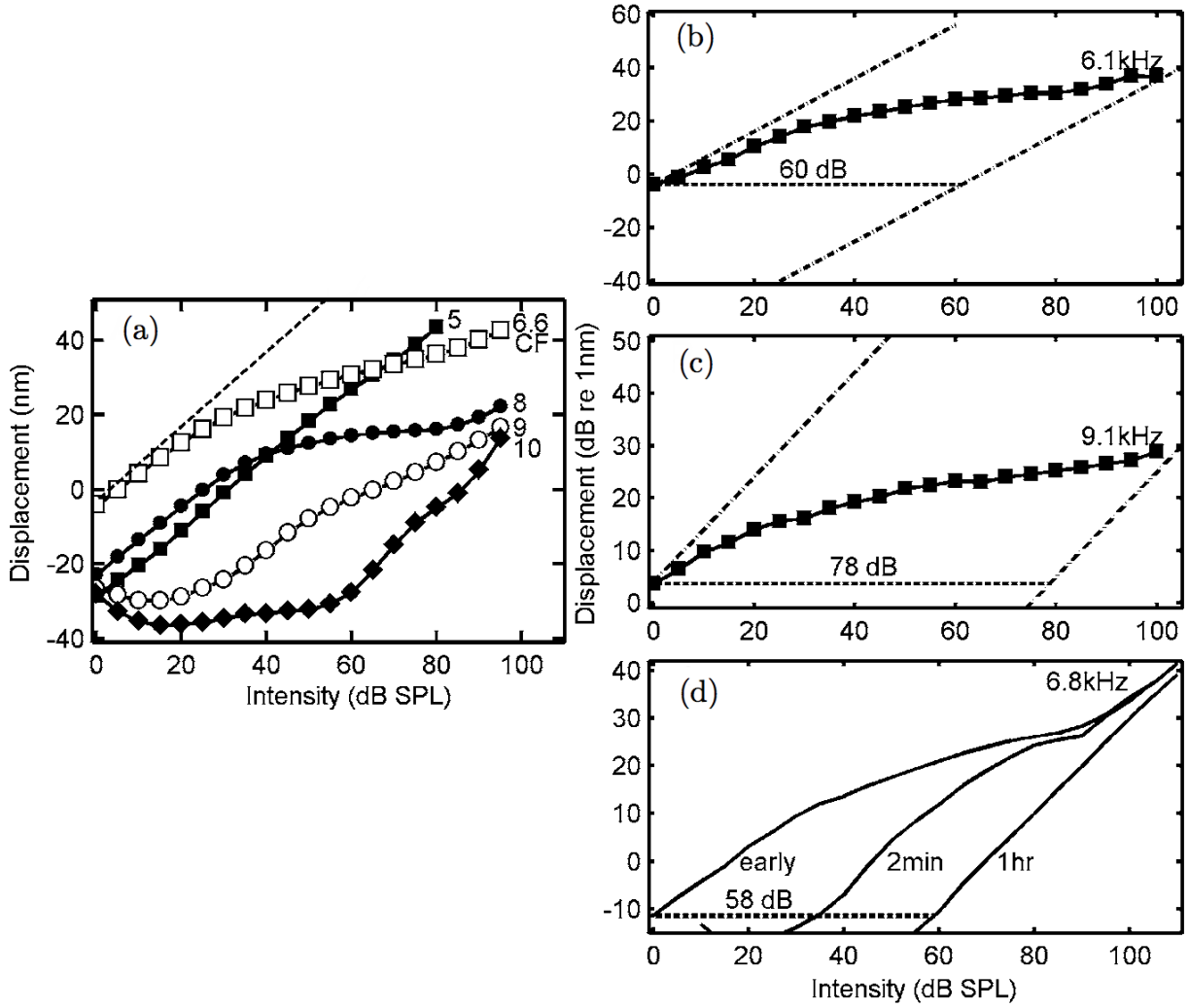
FIG. 2. (a) Basilar membrane vibration amplitude against sound pressure level (plot on a log-log scale) for the chinchilla cochlea at a location corresponding to characteristic frequency (CF) of 6.6 kHz. Each curve corresponds to a different input frequency, as indicated. (b), (c) Similar data obtained from different locations with CF's of 6.1 kHz and 9.1 kHz respectively with stimulation only at the CF frequency in each case. The straight lines have slope 1 and represent linear behavior. (d) Similar result for a location with CF 6.8 kHz for which a treatment has been made which (progressively, over the course of an hour) prevents the function of the active process. Reproduced from Ref. 2 with permission)
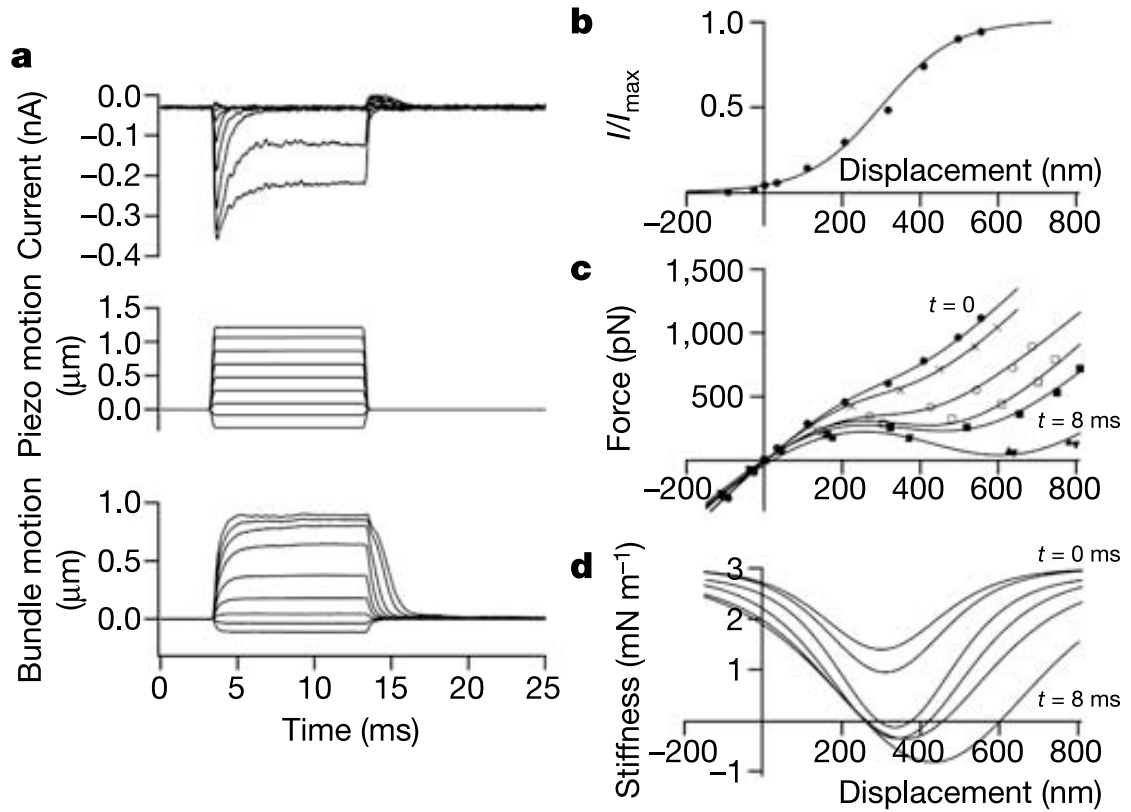
6

FIG. 3. Mechanical properties of the OHC hair bundle. (a) MET currents in a P11 rat for stimulation with flexible fiber (top); also shown are the movements of the fiber end attached to the piezo (middle) and of the hair bundle (bottom). (b) Peak MET current (f) versus displacement (data points) fitted with a Boltzmann relation. (c) Force-displacement plots at successive times (t) after peak current: $t = 0$ (filled circles), 0.07, 0.27, 0.47, 0.67, 3.9, 8ms (filled triangles); theoretical fits using the Boltzmann relation from (b). (d) Slope stiffness of the bundle from differentiating fits in (c). Reproduced from Ref. 3 with permission.

displacements, the force-displacement curve (shown in panel(c)) is approximately linear. Note also from panel (b) how the nonlinear hair bundle behavior correlates with the current flowing into the hair cell body. For all but the largest two stimulations the current flow only occurs as, or shortly after, the bundle moves. During the constantly displaced phase, the current rapidly resets to approximately zero. Careful consideration of the forces involved in the stimulation procedure[3] leads one to the conclusion that the two largest stimulations

in Fig. 3(a) are beyond those that would occur in normal hearing. These observations thus suggest that except for extremely (possibly unphysiologically) large stimulations of the hair bundle, current flow is more a function of hair bundle velocity than of hair bundle position. Finally, the observations do not indicate any intrinsically oscillatory response of the hair bundle to non-oscillatory input.

III. THE HOPF OSCILLATOR MODEL

The two-variable ordinary differential equation (ODE) system which is the normal form of a Hopf bifurcation was first suggested by Eguiluz *et al.*[6] as a suitable phenomenological model for the active dynamics of the organ of Corti. Appealing to the theory of centre manifolds and normal forms (see, e.g., Ref. 7), such an unforced model is guaranteed to capture the low-amplitude dynamics of any smooth system that is on the verge of the onset of self-sustained limit cycle oscillation. The novel feature in the so-called Hopf oscillator model is that this equation is embellished with a forcing term, which represents the input to the OHC from the surrounding BM and fluid. Such a model equation is usually written in the complex form

$$\dot{x} = (\alpha + i\omega_0)x - \sigma x|x|^2 + Fe^{i\omega t}, \qquad x \in \mathbb{C}, \tag{1}$$

where α, ω, and ω_0 are real parameters, while F and σ are in general complex. Without loss of generality (by the transformation $x \mapsto x/\sqrt{|\mathrm{Re}(\sigma)|}$) we can assume that $|\mathrm{Re}(\sigma)| = 1$. The imaginary part of σ affects the frequency but not the amplitude of oscillations, since in polar coordinates ($x = r\cos\theta$, $y = r\sin\theta$) Eq. 1 becomes $\dot{r} = \alpha r + \mathrm{Re}(\sigma)r^3 + \mathrm{Re}(F)\cos(\omega t - \theta) - \mathrm{Im}(F)\sin(\omega t - \theta)$ and $r\dot{\theta} = \omega_0 r + \mathrm{Im}(\sigma)r^3 + \mathrm{Im}(F)\cos(\omega t - \theta) + \mathrm{Re}(F)\sin(\omega t - \theta)$. Furthermore, in the limit $F \to 0$ it is further possible to argue[7] that $\sigma = \pm 1$ without loss of generality. Hence we shall assume $\sigma = \pm 1$ in our numerical investigations for simplicity.

The variable x has been equated with the Fourier component of the basilar membrane displacement at the forcing frequency[8], such that the magnitude of x is the amplitude of the basilar membrane motion. The real parameters F and ω then represent the amplitude and

8

frequency of an incoming wave of pressure difference between the two sides of the organ of Corti. The Hopf oscillator itself is assumed to have natural frequency ω_0, damping α and a nonlinearity coefficient σ. The so-called supercritical case $\text{Re}(\sigma) > 0$ is usually assumed as this leads to small-amplitude limit cycles as α is increased through zero. The sub-critical case $\text{Re}(\sigma) < 0$ leads to growth without bound for large enough initial conditions when α is negative, due to the presence of an unstable limit cycle.

The huge advantages of the Hopf oscillator model are its simplicity, and the fact that it exhibits each of the four features mentioned at the start of this paper; amplification, sharp tuning, compressive nonlinearity and a possible explanation for otoacoustic emissions as a self-excited limit cycle for $\alpha > 0$. In particular, it is easy to show[6] that if $\alpha = 0$ and $\omega = \omega_0$ then the compressive nonlinearity obeys precisely the 1/3-power law that has been argued to be a universal feature. We note that there is evidence[9] that coupled sub-critical Hopf oscillators can produce stronger compression than a single oscillator. On the other hand, a clear weakness of the model is that this result requires precise tuning of two parameters at *each* location along the cochlear partition. It has been suggested[10] that there is an *excitable* feedback process that might adjust each organ to this codimension-two point in parameter space, with any mild over-adjustment so that $\alpha > 0$ causing limit cycle oscillations that emerge as otoacoustic emissions. However, such a mechanism has not yet been identified experimentally.

To test the efficacy of the model (1), we have run a series of direct numerical simulations. The results are shown in Fig. 4. The four panels show results for different damping parameters α. Panels (a) and (b) refer to the case $\alpha < 0$ in which the unforced model has a stable equilibrium. Panel (c) is at the stability boundary $\alpha = 0$ (although the nonlinear terms lead to a weakly stable equilibrium), and panel (d) is for the case when the unforced equilibrium is unstable and is surrounded by a small-amplitude limit cycle.

It can be seen from the figure that in most cases the response increases linearly for small F, then reaches a transition point, beyond which the amplitude varies as the 1/3-power of F. Only for precisely $\omega = 1$, $\alpha = 0$ (the thickest line in panel (c)) does the 1/3-power law
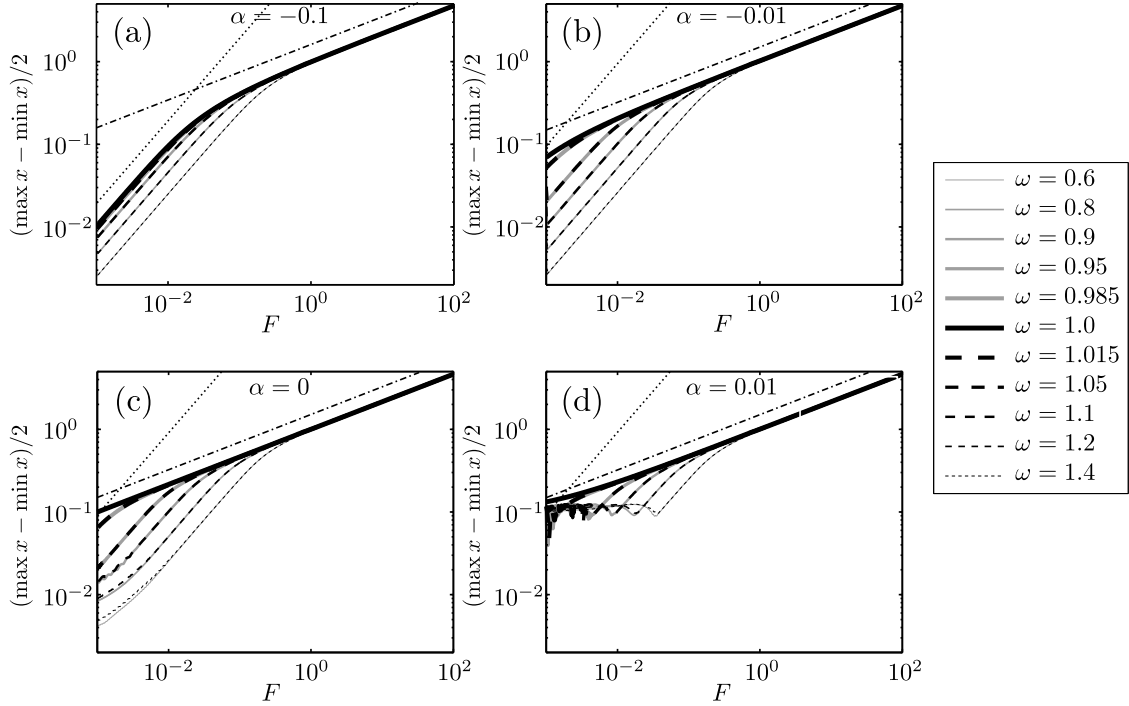
9

FIG. 4. The response of the Hopf oscillator (1) with $\sigma = 1$ and $\omega_0 = 1$. Panels (a)—(d) show response curves (on a log-log scale) of maximum of $|x|$ (after ignoring transients) against sound input amplitude F for a range of different forcing frequencies ω. The values of α used are (a) -0.1, (b) -0.01, (c) 0 and (d) 0.01. The dotted lines have unit slope while the dash-dotted lines have slope $1/3$. We used the `ode15s` solver of MATLAB with relative and absolute tolerances of 10^{-12}.

extend right down to zero input amplitudes. For $\alpha > 0$, the unforced response is already an oscillation, hence the amplification at $F = 0$ is infinite (as the response has a non-zero amplitude when the stimulus amplitude is zero). This self-sustained oscillation can interact nonlinearly with the forcing to produce complex vibrations, which can be either phase locked to a high-period limit cycle or genuinely quasi-periodic. These dynamics are reflected in 'beating' or 'mode locking' effects that lead to the dips in the graphs in Fig. 4(d) of output amplitude against sound input level F, for small F. One extra positive feature of the Hopf oscillator model inherent in the above simulations is that the compressive nonlinearity for sufficiently high input levels does not rely on precise tuning to the codimension-two point

$(\alpha, \omega) = (0, \omega_0)$.

It is understood that the unforced Hopf oscillator is a normal form for a local bifurcation, hence it is thought to be valid for a small range of forcing amplitudes around the equilibrium. So we do not expect such a small amplitude model to show the correct compression over the full amplitude range of 120dBs that humans can observe. Indeed, the model gives the 1/3-power law up to arbitrary large forcing amplitudes, whereas the data in Fig. 2 shows an eventual linear response. Also, the explanation of otoacoustic emissions as spontaneous oscillations on the unstable side of a Hopf is convenient, but it is not the only possible explanation. Indeed, the source of the instability need not necessarily be local, but could also be caused by longitudinal coupling[11] (which results in a Hopf bifurcation as an emergent feature). For example, it has been proposed that spatial inhomogeneities along the basilar membrane in a linear model can cause spontaneous otoacoustic emissions[12–14].

IV. CUSP BIFURCATION MODEL

In the same spirit as the Hopf bifurcation model we can suggest a simpler equation that exhibits 1/3-power compressive nonlinearity for large amplitude. Moreover, this model aims to capture the negative stiffness of the hair bundle that is inherent in Fig. 3(d) without introducing frequency selective hair bundle, as mammalian hair bundles do not appear to be tuned. In essence, the 1/3-power compression comes from the presence of a cubic nonlinearity. So as a simplification, we can model the hair bundle as a cubic spring. Moreover, in line with the temporal relaxation inherent in Fig. 3(a), we suppose that the spring is driven principally by viscous damping rather than inertia.

A simple model equation for the displacement x of such a single spring then reads

$$\dot{x} = \alpha + \beta x - \sigma x^3 + F \sin \omega t, \qquad x \in \mathbb{R}, \tag{2}$$

where α is a static bias, β is the ratio of linear stiffness to damping, σ is a nonlinear stiffness ratio, and, as in (1), F and ω represent the amplitude and frequency of a pure tone sound input. Note that the unforced ($F = 0$) version of equation (2) with α and β thought of

11

as independent parameters is the normal form for the so-called cusp bifurcation, see e.g. Ref. 7. Such a normal form is a universal two-parameter unfolding of any system in the neighborhood of a point of the onset of bistability. By scaling x, the nonlinear parameter σ can be reduced to ± 1, and by changing the sign of x, β and α, without loss of generality we can assume $\sigma = 1$. The bifurcation diagram of the unforced system is depicted in Fig. 5(a).

The numerical response diagram can be seen in Fig. 5(b)-(d) which confirm this approximate scaling result. Dashed curves represent unstable vibrations that are not observable by direct numerical simulation. Note that in Figs. 5(c),(d) there are multiple curves indicating coexisting stable vibrations for smaller forcing amplitudes.

The dependence of the response curves on the forcing frequency can be seen in Fig. 6. The result for the model (2) in Fig. 6(a) does not show much sensitivity to ω, because of the lack of tuning in the model. Now tuning could emerge from the passive resonance of the basilar membrane. Thus, in order to account for tuning in the local model, we couple equation (2) to a single degree of freedom oscillator, as described by the system

$$\ddot{z} = -2\zeta\omega_0\dot{z} - \omega_0^2 z + F\sin\omega t, \qquad (3)$$

$$\dot{x} = \alpha + \beta x - \sigma x^3 + \dot{z}.$$

Here, z represents the internal variable of the passive tuning mechanism, with CF ω_0 and damping ratio ζ, while x represents the active BM response.

The results from numerical investigaton of Eq. (3) can be seen in Fig. 6(b). Note that they show a more varied response for different frequencies similar to that of the Hopf oscillator (1) in the previous section. We also note that in order to achieve the 1/3 compressive nonlinearity one does not need to be exactly at the cusp bifurcation point ($\alpha = 0$, $\beta = 0$); the model works well for broad ranges of parameter values. In a sense this is a similar situation with the Hopf bifurcation normal form that requires $\omega = \omega_0$ and $\alpha = 0$ to be precisely at the bifurcation point for the given input frequency. In essence, though, both models are equally good as they show the 1/3-power law for sufficiently large amplitudes. This is not due to the local bifurcation, but to the fact that both models have a cubic nonlinearity.
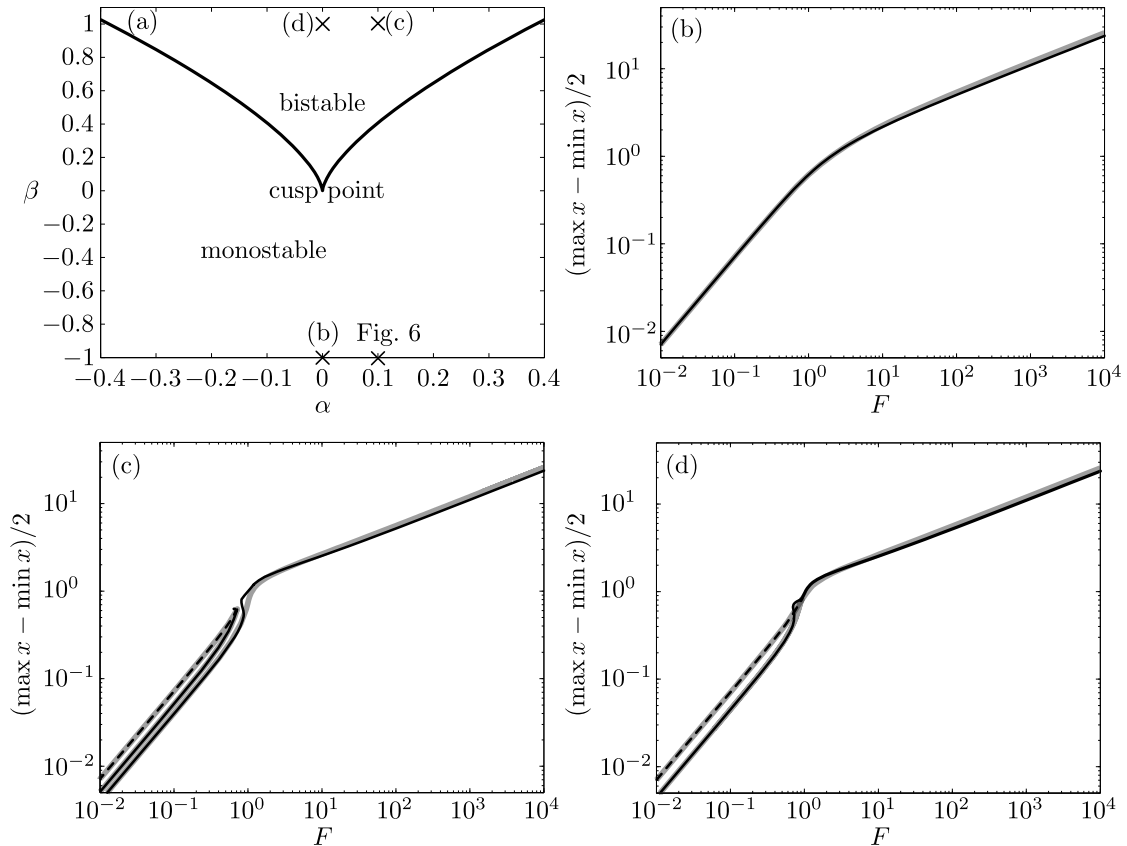
12

FIG. 5. (a) Two-parameter plot of the bifurcation diagram of the cusp normal form (2) with $F = 0$ and $\sigma = 1$. Note that the cusp point occurs for $\alpha = \beta = 0$. (b)—(d) The vibration amplitude of the cusp normal form model (ignoring the DC component a_0) as a function of the input amplitude F for a variety of input frequencies ω. Thick shaded lines correspond to numerical data (computed using PDDE-CONT[15]), and black lines represent the harmonic balance approximation (A1), (A2) or equivalent formulae for $\alpha = 0$ (see Appendix A). The dashed curves indicate unstable vibrations that are 'invisible' in direct simulations. The parameters are: (b) $\alpha = 0$, $\beta = -1$ (c) $\alpha = 0$, $\beta = 1$ and (d) $\alpha = 0.1$, $\beta = 1$.

Interestingly, for the experimentally fitted parameter set in Fig. 1 of Ref. 16, the unforced problem is as close to a cusp bifurcation point as it is to a Hopf bifurcation.

We note here that both the Hopf and cusp models share the disadvantage that they are phenomenological; that is, they are motivated more by (some) features of experimental data
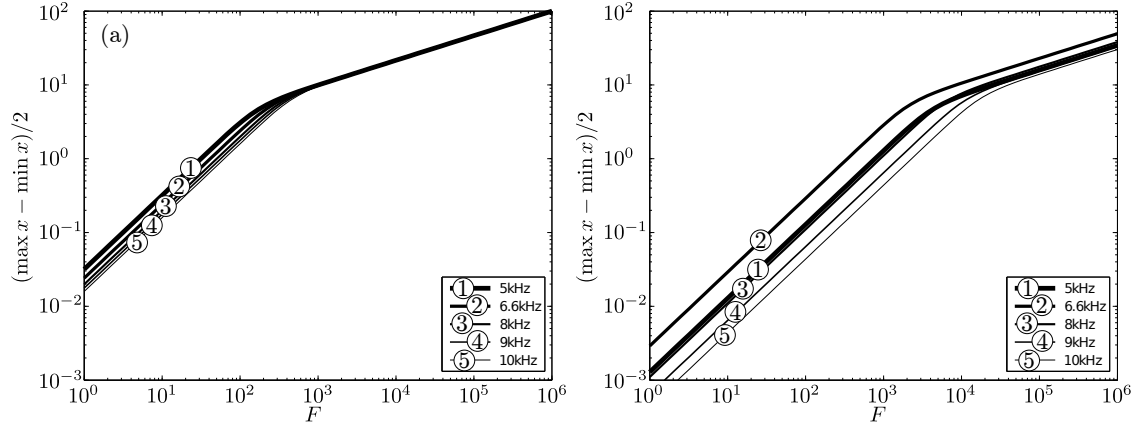
FIG. 6. The response of the cusp bifurcation model for equation (2) in panel (a) and for (3) in panel (b), with $\alpha = 0.1$, $\beta = -1$ and $\sigma = 1$. The additional parameters for (3) are $\zeta = 0.1$ and $\omega_0 = 6.6 \times 2\pi$ with time measured in milliseconds.

than by the underlying biophysics of the cochlea. We now proceed to discuss models that are physiologically inspired, and robust to this criticism.

V. PHYSIOLOGICAL MODEL WITH BOTH ACTIVE HAIR BUNDLE MOTILITY AND SOMATIC MOTILITY

We first consider a model of active cochlear mechanics which includes both somatic motility and active hair bundle motility. This description illustrates the interplay between these two processes as a result of the current flowing through the outer hair cell, and also due to mechanical coupling to other structures in the cochlear partition. Moreover, this depiction shows how somatic motility results in feedback to the hair bundle and to the basilar membrane.

Ó Maoiléidigh & Jülicher[4] use a model for active hair bundle motility illustrated in Fig. 7. The figure shows two stereocilia (the cilia of the hair bundles) which are connected to each other by a tip-link, modeled as a linear spring with stiffness k_{gs}. The coordinate x_{hb} is the position of the hair bundle and x_{a} is the position of the adaptation motor inside the hair bundle. The tip-link is attached to a mechanically sensitive ion channel that changes its

14
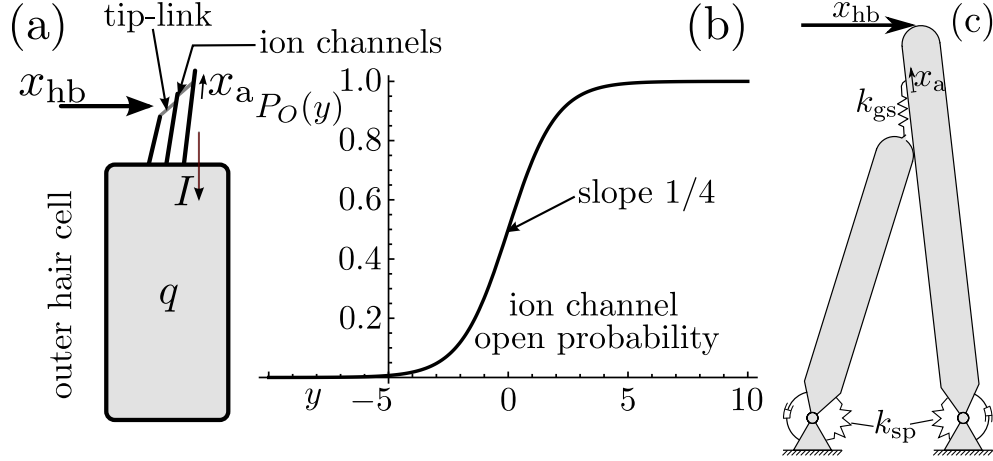
FIG. 7. Schematic description of hair bundle mechanics. (a) The transverse geometry of an OHC showing rows of cilia displaced by an angle x_{hb} connected by elastic tip links of stiffness k_{gs}. The links are pinned to the end of the shorter hair, and are free to move a distance x_{a} up and down the longer hair through the action of myosin motors. The stretching of the tip link controls the open probabilities of an ion channels that cause depolarizing current I to flow into the hair cell body. The open probability follows the Boltzmann-like function depicted in panel (b), see equation (5). Panel (c) shows more details of the mechanics of two adjacent cilia.

configuration as the channel opens and closes, thereby changing the total length of the tip link by an amount D. The ion channel has a sigmoidal-shaped open probability function (of displacement). The tip-link is also attached to a myosin-based adaptation motor that tenses the tip-link and is controlled by the local calcium concentration, which in turn depends on the state of the ion channel. The adaptation motor can exert a maximal force f_{max}, and has a sensitivity S to calcium through the open probability of the ion channel. In the model the mass of the hair is neglected because the dynamics is over-damped, with time scales λ for the hair bundle and λ_a for the adaptation motor.

Somatic motility is described to linear order using the piezoelectric relationships between (i) the charge inside the outer hair cell and the force exerted by the cell, and (ii) the extension of the cell and the change in transmembrane electric potential. The linearity of

15

these relationships holds for small physiological displacements. The complete description of cochlear mechanics includes terms representing the mechanical force on the hair bundle due to charge movement through the outer hair cell resulting from somatic motility, as well as changes in the current through the outer hair cell due to the displacement of the hair bundle.

In what follows we shall consider a simplification of the Ó Maoiléidigh and Jülicher model. The main nonlinear parts of their model can thus be written:

$$\lambda \dot{x}_{\mathrm{hb}} = -k_{\mathrm{gs}} \left[x_{\mathrm{hb}} - x_{\mathrm{a}} - D P_{\mathrm{O}}(\Delta(x_{\mathrm{hb}} - x_{\mathrm{a}} - \delta)) \right] - k x_{\mathrm{hb}} - \gamma_1 p q + \mu_{\mathrm{hb}} F \cos \omega t,$$

$$\lambda_{\mathrm{a}} \dot{x}_{\mathrm{a}} = k_{\mathrm{gs}} \left[x_{\mathrm{hb}} - x_{\mathrm{a}} - D P_{\mathrm{O}}(\Delta(x_{\mathrm{hb}} - x_{\mathrm{a}} - \delta)) \right] - \gamma f_{\max} \left[1 - S P_{\mathrm{O}}(\Delta(x_{\mathrm{hb}} - x_{\mathrm{a}} - \delta)) \right], \quad (4)$$

$$\dot{q} = I_{\mathrm{hb}} P_{\mathrm{O}}(\Delta(x_{\mathrm{hb}} - x_{\mathrm{a}} - \delta)) - \frac{g}{C_{\mathrm{eff}}} Q - g p \gamma_1 x_{\mathrm{hb}} - g p \alpha_1 F \cos \omega t,$$

where

$$P_{\mathrm{O}}(y) = \left(1 + \mathrm{e}^{-y} \right)^{-1} \tag{5}$$

is the open probability function of the ion channels. The simplifiction of a larger model eliminated variables including the BM position that can be recovered by the simple equation

$$x_{\mathrm{bm}}(t) = 11.72 \left[\frac{\mathrm{nm}}{\mathrm{Pa}} \right] F \cos \omega t + 135.52 \left[\frac{\mathrm{nm}}{\mathrm{pC}} \right] q(t) + 1.276 \left[- \right] x_{\mathrm{hb}}(t). \tag{6}$$

The parameters in the charge equation are the maximum current I_{hb} that flows through the ion channels, the piezoelectric constant p, the leakage resistance g and the capacitance C_{eff} of the OHC. The stiffness parameter k contains both the hair bundle stiffness k_{sp} and structural stiffness of the organ of Corti; γ is a geometric factor. The pressure difference through the cochlea cross-section is transformed to a force on the hair bundle by μ_{hb}. The parameters γ_1 and α_1 are constants determined by the geometry of the organ of Corti.

Considerable effort[4,17] has been expended in finding physiologically plausible values for each of the parameter values in the model. Specifically, in what follows we shall follow Ó Maoiléidigh and Jülicher[4], and take parameter values as given in Table I. Note that we allow $f_{\max}$, S and D to make variations from the values in Ref. 4, in order to explore the behaviour of the model under variation of parameters.
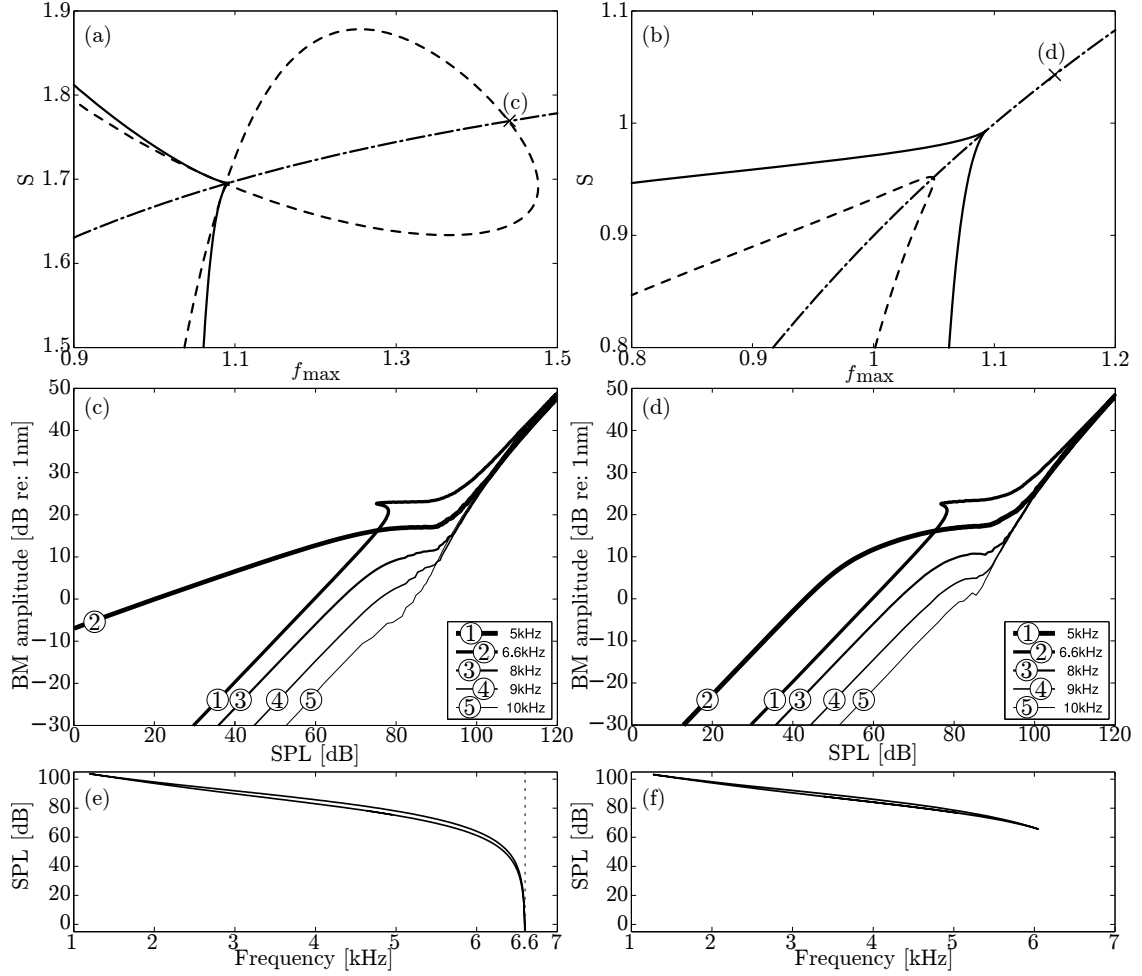
FIG. 8. (a),(b) Bifurcation diagrams of equation (4) at parameter values given in Tab. I, with $F = 0$ as the two parameters $f_{\max}$ and S are allowed to vary for $D = 60\,\mathrm{nm}$ and $D = 36\,\mathrm{nm}$, respectively. Continuous lines represent fold bifurcations. The dash-dotted lines show equilibria with $P_O = 1/2$. (c) The response of the forced model for $D = 60\,\mathrm{nm}$ near a Hopf bifurcation; and (d) far from a bifurcation curve $D = 36$. (e),(f) The locations of the hysteresis of response in frequency and SPL for $D = 60\,\mathrm{nm}$ and $D = 36\,\mathrm{nm}$, respectively.

A. Bifurcation analysis: Hopf and cusp bifurcations

The unforced dynamics of the model can be characterized by its bifurcation diagram, which we have computed using numerical continuation methods[15]. The results are presented in Fig. 8(a)–(b). It can be seen from the figures that for both values of D there are two

17

fold bifurcations that connect at a cusp point. Inside the wedge-shaped parameter region between the two fold bifurcations there are two stable equilibria, outside it there is just one. In addition, for D sufficiently large, a loop shaped curve of Hopf bifurcations occurs, such that the equilibrium becomes unstable inside the loop. Depending on the criticality of the Hopf bifurcation a stable limit cycle exists inside the loop or also in its small outer neighborhood in the subcritical case. The Hopf bifurcation curve on both sides of the cusp point meets the fold curve at a fold-Hopf bifurcation, an unfolding of which is likely to signal the presence of further bifurcation curves[7].

The Hopf loop disappears from the bifurcation diagram at a so-called codimension-three Hopf-cusp bifurcation that occurs as we vary D. We shall show below that decreasing D below this critical value, and hence eliminating the Hopf bifurcation, still results in a compressively nonlinear response.

First, to find the codimesion-three point, note that the cusp bifurcation always occurs on the line where equation (4) has a symmetry, that is, where there is an equilibrium with $P_O = 1/2$. In fact, the two-parameter bifurcation diagram in Fig. 8(a) is symmetric about this dash-dotted line, independently of D. So in order to find the critical codimension-three point, we need to find a condition where the two fold-Hopf points meet and occur for an equilibrium at $P_O = 1/2$. This can be done by restricting the system to $P_O = 1/2$ and then stipulating that the characteristic polynomial of the Jacobian of (4) must have vanishing constant and second-order terms. This condition is equivalent to requiring for a pair of purely imaginary and a single zero root of the system at the equilibrium. A routine calculation allows us to find the unique set of parameters and coordinate values for the codimesion-three Hopf-cusp bifurcation, that is,

$$x_{\mathrm{hb}} = -66.6283\,\mathrm{nm},\ x_{\mathrm{a}} = -101.823\,\mathrm{nm},\ q = 0.794324\,\mathrm{pC},$$

$$f_{\max} = 1.09309\,\mathrm{nN},\ S = 1.07164\ \text{and}\ D = 38.6783\,\mathrm{nm}.$$

Therefore, values of $D < 38.6783\,\mathrm{nm}$ will result in no Hopf bifurcations outside the bistable region. A bifurcation diagram without the Hopf loop can be seen in Fig. 8(b) for $D = 36\,\mathrm{nm}$.

B. Forced dynamics

In order to study the forced dynamics we rescale the forcing frequency in equation (4), so that it is most sensitive at 6.6 kHz, the CF for the data in Fig. 2. The most sensitive frequency ω_{sens} can be computed approximately from the complex eigenvalues of the Jacobian of (4), and is the imaginary part of this eigenvalue. Then we rescale the frequency so that when we assume 6.6 kHz forcing we are in fact forcing at $\omega_{\text{sens}} \approx 4 \times 2\pi$ ms^{-1}. The forced response curves are shown in panels (c)—(d) of Fig. 8 for the Ó Maoiléidigh & Jülicher model (4).

In figures 8(c) and 8(d) the system is tuned such that the equilibrium occurs for $P_O = 1/2$. It can be argued from an evolutionary point of view that $P_O = 1/2$ is preferable as this leads to maximum sensitivity of the hair bundles. In figure 8(c) we used the same parameters that were used to test the nonlinear behaviour in Ref. 4. The result is directly comparable to Fig. 2(a) since it uses the same quantities and units. The qualitative behaviour is strikingly similar to that of the experimental data. However, one extra feature apparent. For the 5 kHzfrequency, the response displays a hysteresis or a jump in amplitude, which is not seen in the experiment. This jump is present but less apparent in Fig. 5 of Ref. 4.

To demonstrate that being near the Hopf bifurcation is not necessary for compressive nonlinearity we used a parameter set ($D = 36$ nm, $f_{\text{max}} = 1.15$ nN and $S = 1.04305$) where the Hopf bifurcation is removed from the monostable parameter region of the system. The result of the computation (Fig. 8(e)) is rather similar to Fig. 8(d) with the difference that the amplifiction is significantly lower. However, there is still 40dB between the 6.6kHz and 10kHz response at low SPLs. This is an indication that the Hopf bifurcation is not the ultimate feature of the system that produces the compressive nonlinearity.

In figure 8(e)—(f) we mapped out the region where the hysteresis takes place in the parameter region of forcing frequency and amplitude for our two cases. Notice that lower than CF frequencies are affected and that the hysteresis occurs at higher amplitude as the forcing frequency decreases. While removing the Hopf bifurcation from the monostable

region reduces the region of hysteresis we found that the phenomena could not be removed without compromising the overall behaviour of the model.

Given that equation (4) produces results that give plausible agreement with experimental data under variation of parameters (e.g. D) which qualitatively change the structure of the underlying dynamics (e.g. the presence or not of Hopf bifurcations), we are interested to investigate which are the key features of the mathematical model. In what follows, therefore, we shall try to capture the essence of the model with the aim of providing further insight into which physiological features might be the most important, and which parameter values should be the most critical to measure accurately.

C. A simplified model

When analyzing the forced response of (4), it would appear that it is possible to neglect all the nonlinearity of the hair bundle mechanics. We suggest that the term $I_{hb}P_O$, occurring in equation (4) for $\dot{q}$ is sufficient to produce realistic compressive nonlinearity. Linearizing the open probability function at the equilibrium $P_O = 1/2$ in the equations for x and x_a lead to a forced damped oscillator which is coupled to a capacitor with charge q. To ensure $P_O = 1/2$ we fix the sensitivity

$$S = \frac{Dk_{gs} + 2k_{gs}\delta}{f_{max}\gamma} + 2.$$

Using the transformation

$$x_{hb} = y + \frac{2\lambda_a \dot{y}}{f_{max}\gamma\Delta + k_{gs}(\delta\Delta + 2)}, \quad x_a = y$$

we write down the simplified model

$$\ddot{y} = -2\zeta\omega_0\dot{y} - \omega_0^2 y - \frac{p\gamma_1}{k}\omega_0^2 q + \frac{\omega_0^2 \mu_{hb}}{k}F\cos\omega t,$$

$$\dot{q} = -gp\gamma_1 y - c_2\dot{y} - \frac{g}{C_{eff}}q + I_{hb}P_O(\Delta\dot{y}) - gp\alpha_1 F\cos\omega t. \tag{7}$$

Within the model ω_0 is the CF for the cross-section of the cochlea in question and ζ is the relative damping factor. Note that P_O depends on $\dot{y} = \dot{x}_a$. This is the result of the

20

transformation and matches the observation inherent in the data in Fig. 3 that the current flow depends chiefly on hair bundle velocity, rather than displacement.

The rest of the parameters are transformed as

$$\omega_0^2 = \frac{k(f_{\max}\gamma\Delta + k_{\mathrm{gs}}(\delta\Delta + 2))}{2\lambda_{\mathrm{a}}\lambda},$$

$$2\zeta\omega_0 = \frac{k_{\mathrm{gs}}\lambda_{\mathrm{a}}(4 - D\Delta) + 2\lambda(f_{\max}\gamma\Delta + k_{\mathrm{gs}}(\delta\Delta + 2)) + 4k\lambda_{\mathrm{a}}}{4\lambda_{\mathrm{a}}\lambda},$$

$$c_2 = \frac{\lambda_{\mathrm{a}}(I_{\mathrm{hb}}\Delta - 4g\gamma_1 p)}{2(f_{\max}\gamma\Delta + k_{\mathrm{gs}}(\delta\Delta + 2))}.$$

Figure 9 shows the forced response curves for the simplified model (7) using the parameter
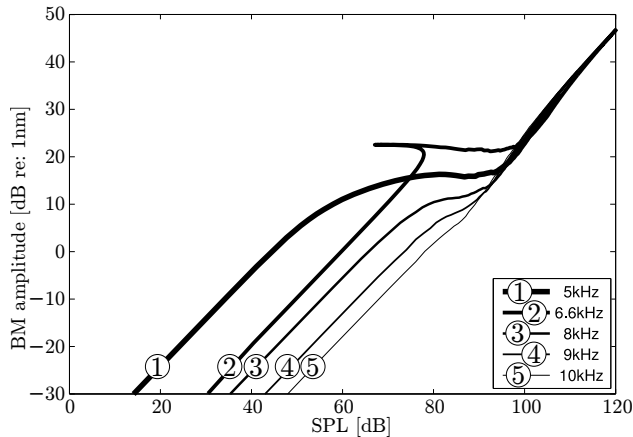
FIG. 9. Response of the simplified model (7). Parameters are the same as in Fig 8(e).

values in Tab. I with the exception of $D = 36\,\mathrm{nm}$ and $f_{\max} = 1.15\,\mathrm{nN}$, again with CF scaled to 6.6 kHz. It can be seen from the figure that the model behaves in essentially the same way as equation (4), it even capure the bistable behaviour of Fig. 8(e) even though most nonlinearity is removed. We note that the damping coefficient ζ is negative for $f_{\max} < 1.209\,\mathrm{nN}$.

The system (7) loses its stability for $f_{\max} < 1.04\,\mathrm{nN}$ with a characteristic root passing through 0. We note that this stability loss is not a generic bifurcation, because no extra solution is created before or after this parameter value. The already unstable system also undergoes supercritical Hopf bifurcation at $f_{\max} \approx 0.9574\,\mathrm{nN}$, which has no effect on the overall dynamics.

VI. MODEL WITH NONLINEAR TRANSDUCTION CURRENT AND ELECTROMOTILITY

It should be remembered that the measured data in Fig. 2 are the vibration amplitude of the BM, not the charge in the OHC, nor the deflection of hair bundles. The precise mechanism of feedback of somatic motility to the BM is likely to be through the Deiters' cells. With this in mind, we shall propose here another model that aims to capture only these features.

Since it is possible to capture the nonlinear compression in a model without active hair bundle motility we propose a modified version of the full description of organ of Corti mechanics given in Ref. 4. The model is described conceptually in Fig. 10, illustrating how the motion of the hair bundle $x_{\mathrm{hb}}(t)$ is coupled to that of the BM deflection $x_{\mathrm{bm}}(t)$ through the excess charge $q(t)$ in the OHC.

In our model the hair bundle is coupled to the basilar membrane through a simple mechanism that neglects the inertia of the HB and assumes a passive HB mechanics. Hence, we only need to model the transduction current that causes the hair cell to expand and contract. As can be seen in Fig. 3, the transduction current peaks at the onset of the displacement stimulation and it settles back to almost zero assymptotically. This current is accurately modeled by Tinevez et al.[17]. However, we aim for a passive hair bundle, therefore our model can be simpler. We assume an exponential decay with time constant κ and an almost complete adaptation. We also suppose that there is an adaptation variable x_{a} that is linearly adapting to the hair bundle displacement x_{hb}. The transduction current flowing through the ion channels is then a function (P_{O}) of both the speed and the position of the adaptation variable ($\alpha x_{\mathrm{a}} + \beta \dot{x}_{\mathrm{a}}$), where $\beta > \alpha$ in order to capture the observation that the current is more a function of bundle velocity than displacement. Hence we reach a simple transduction current model

$$\dot{x}_{\mathrm{a}} = -\kappa(x_{\mathrm{a}} - x_{\mathrm{hb}}), \tag{8}$$

$$I = -P_{\mathrm{O}}(\Delta(\alpha x_{\mathrm{a}} + \beta \dot{x}_{\mathrm{a}})), \tag{9}$$

22
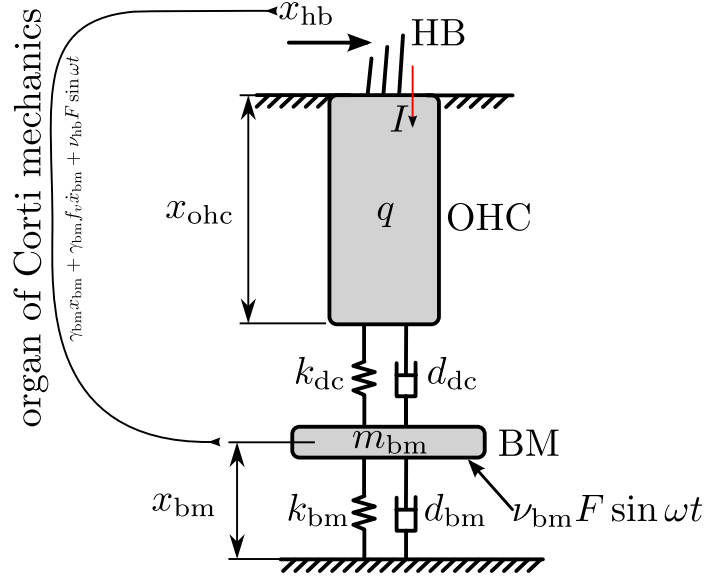
FIG. 10. Schematic description of a somatic motility model with feedback to the basilar membrane. The basilar membrane (BM) is coupled to the bone structure of the cochlea and to the OHC through the Deiters' cells. The pressure difference wave $\nu_{bm} F \sin \omega t$ causes the BM to vibrate with amplitude $x_{bm}(t)$ A combination of the fluid pressure difference and the BM motion forces the hair bundle, which cause ion channels to open that conduct ion currents I into the OHC. The outer hair cell changes its length in proportion to its excess charge q. The Deiters' cells then feedback to the BM the force exerted by the OHC.

where $P_O(\cdot)$ is as defined in (5). The response of such a simple adaptation function to step displacements of different magnitude is shown in Fig. 11. Note the qualitative agreement of such a function to the data in Fig. 3(a).

In this model, the BM is modeled as a linear oscillator with natural frequency ω_0, the CF of the longitudinal position in question, and damping ratio ζ. The BM is also coupled to the OHC through the Deiters' cells that are again represented by a spring and a damper. This force is represented by the term $\omega_0^2 f_q q$. The detailed derivation of the mechanics can be found in Appendix B.

We suppose that the excess charge q in the hair cell leaks at rate γ and that the hair cell expands and contracts from its equilibrium length in direct proportion to the excess charge.

23
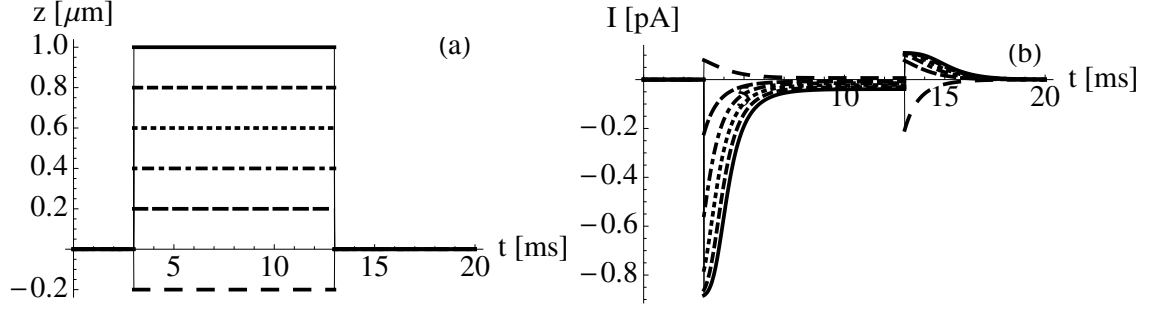
FIG. 11. Adaptation of the transduction current in the hair bundle. (a) The applied displacement steps $x_{\mathrm{hb}}(t)$ applied to the hair bundle. (b) (b) The corresponding transduction current $I(t)$ given by (9). The parameters used are $\kappa = 1\mathrm{ms}$, $\alpha = 0.03$, $\beta = 1$ and $\Delta = 7$.

The force of the OHC is calculated as $F_{\mathrm{ohc}} = -k_{\mathrm{ohc}}x_{\mathrm{ohc}} - d_{\mathrm{ohc}}\dot{x}_{\mathrm{ohc}} - pq$, where p is the piezoelectric constant of the OHC. The hair cell is charged by the transduction current I. The hair bundle excitation is driven by the basilar membrane motion $x_{\mathrm{bm}}(t)$ and indirectly by the assumed sinusoidal pressure difference $\nu_{\mathrm{hb}}F \sin \omega t$. This indirect forcing term arises from the derivation in Appendix B, where we assume that the coupled passive BM and hair bundle has a general two degree of freedom mechanics. Even though the indirect forcing by the pressure is small, its effect can be rather large due to the sensitivity of the hair bundle.

Under the above assumptions, the governing set of equations is

$$\ddot{x}_{\mathrm{bm}} = -2\zeta\omega_0\dot{x}_{\mathrm{bm}} - \omega_0^2\left(x_{\mathrm{bm}} - f_q q\right) + \nu_{\mathrm{bm}}F \sin \omega t,$$

$$\dot{x}_{\mathrm{a}} = -\kappa\left(x_{\mathrm{a}} - \left(\gamma_{\mathrm{bm}}x_{\mathrm{bm}} + \gamma_{\mathrm{bm}}f_v\dot{x}_{\mathrm{bm}} + \nu_{\mathrm{hb}}F \sin \omega t\right)\right), \qquad (10)$$

$$\dot{q} = -\gamma q + I_{\mathrm{hb}}P_{\mathrm{O}}(\Delta\dot{x}_{\mathrm{a}}) - P_{\mathrm{O}}(0),$$

where P_{O} is defined as before. The parameters of the model can be seen in Table II.

The unforced model (10) (with $F = 0$) has a unique equilibrium. The stability of this equilibrium can be computed by linearization. The stability chart in terms of the two parameters f_q, f_v is shown in Fig. 12(a). The stable region is bounded a Hopf bifurcation curve (thick solid line). The stable system has two resonances in the grey regions and we assume that the higher resonance frequency is the CF. These two frequencies are close to each other around the point (e).

24
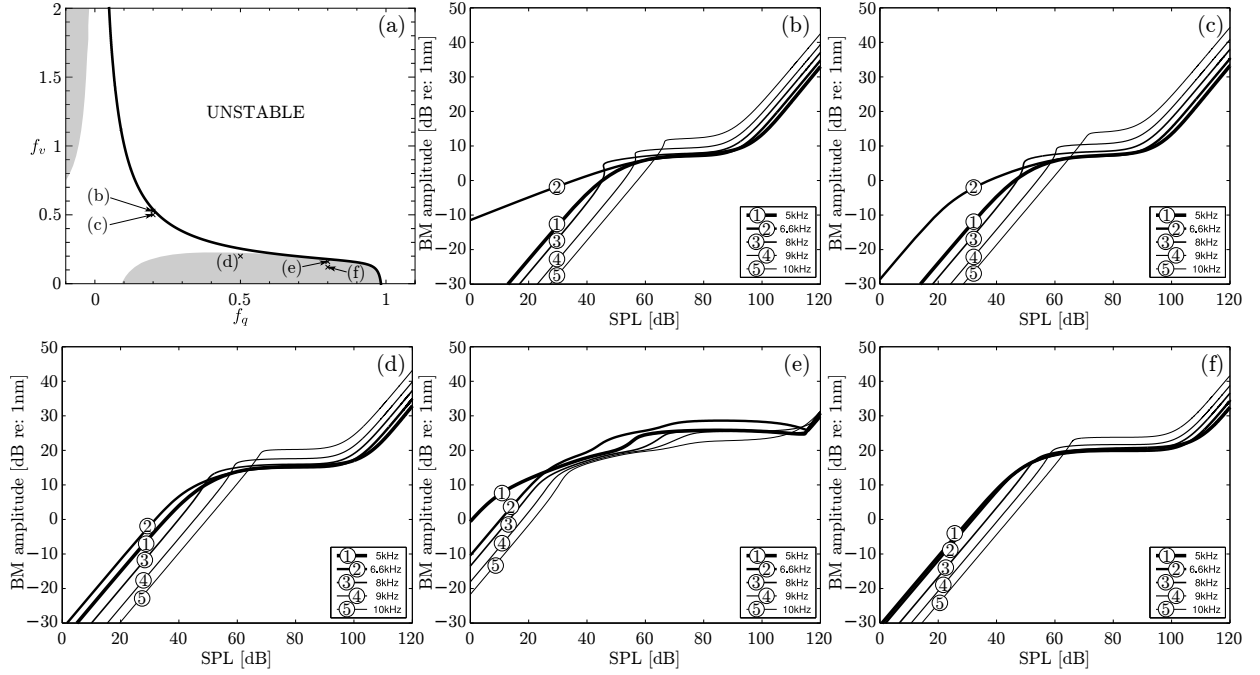
FIG. 12. Panel (a) shows the stability chart of model (10) in terms of the two feedback parameters f_q and f_v. Amplitude response of the model (10) is shown in panel (b) for $f_q = 0.2\,\text{V/N}$, $f_1 = 0.539\,\text{ms}^{-1}$ (c) for $f_q = 0.2\text{V/N}$ $f_v = 0.5\,\text{ms}^{-1}$, (d) for $f_q = 0.5\text{V/N}$ $f_v = 0.2\,\text{ms}^{-1}$, (e) for $f_q = 0.87\text{V/N}$, $f_v = 0.163\,\text{ms}^{-1}$ and (f) for $f_q = 0.87\text{V/N}$ and $f_1 = 0.12$. Other parameters can be found in Table II.

The amplitude response of Eq. (10) is depicted in Fig. 12(b)–(f). Like the models introduced in the previous section, it can be seen in Fig. 12(b) that the amplitude response has a linear region for small forcing amplitudes, a plateau for medium range forcing amplitudes and it tends to be linear again for the highest forcing amplitudes, consistent with the data in Fig. 2. The parameters of Figs. 12(b),(e) are tuned near a Hopf bifurcation, therefore their frequency tuning is better than at other parameters. It is also interesting to note that the two nearby resonances in Fig. 12(e) make the system very compressive and that the 5 kHz curve represents a higher amplitude response than the 6.6 kHz curve. Also, tuning is not evident in Fig. 12(e),(f), because of nearby resonances in the system. As one moves away from the Hopf bifurcation in Fig. 12(c),(d),(f) the linear tuning diminishes however the compression remains. Another difference from the previous models is that hysteresis

25

occurs for frequencies higher than CF.

Many physiological features are omitted from this model. In particular, the active force of the hair bundle is excluded, in favour of the transduction current that drives the BM through the somatic motility of the OHC. This shows that active hair bundle motility is not necessary for compressively nonlinear amplification if the hair bundle is forced by the pressure difference across the cochlear partition due to a passive organ of Corti mechanism.

VII. DISCUSSION

In this paper we have used mathematical modeling and numerical continuation techniques to study the compressive nonlinearity present in the mammalian cochlea. We have assessed various models, including the popular Hopf oscillator model, another phenomenological model inspired by observed hair bundle characteristics, followed by a model based on detailed physiological understanding, with two simplified models that aim to capture some of its key features. One key conclusion from our analysis of these models is that the presence of a Hopf bifurcation is not necessary for a local model to produce results in agreement with experimental data.

We first considered the Hopf oscillator model, Eq. (1), and highlighted several shortcomings. The Hopf oscillator model does not exhibit compression of greater than 1/3-power, nor an ultimately linear region, and so does not compare well with the data shown in Fig. 2. In addition the original motivation for the Hopf model, in which the 1/3-power law is felt right down to zero input, requires delicate two-parameter tuning. Nevertheless, the 1/3-law can still be seen for large input amplitudes without this tuning, although $\alpha > 0$ must be avoided to prevent self-oscillation (although such oscillations may have a role in explaining otoacoustic emissions). However, we should note that there is recent evidence[18] that the presence of noise in the normal form for a Hopf oscillator can give compression levels that are flatter than 1/3.

Next we compared the Hopf oscillator with another phenomenological model, that of a

cusp oscillator, Eq. (2). The output of the cusp oscillator also shows linear response for small input, and 1/3-power compression for larger forcing. Furthermore, it is robust to parameter changes. However, the key feature shared by both the cusp and the Hopf oscillator models, which gives rise to a 1/3-power nonlinearity, is actually cubic nonlinearity.

We then described the physiologically-based model of Ó Maoiléidigh & Jülicher[4], Eq. (4), in which the authors have taken significant care to include physically measurable parameter values. The results are better than either the Hopf or cusp oscillator models, in that there is smaller rate of growth than 1/3 and an eventual linear region for large input.

In order to understand better the key features of the Ó Maoiléidigh & Jülicher model, we pose two simplifications. The first, Eq. (7), consists only of a forced damped oscillator coupled to a capacitor through the open probability function. The results are strikingly similar to those obtained from the full physiologically-based model. Perhaps most interestingly, this model contains neither a Hopf bifurcation nor a cusp, and still produces results that are in reasonably good agreement with the data in Fig. 2.

Finally, we proposed a second simplification of the Ó Maoiléidigh & Jülicher model, Eq. (10), omitting active hair bundle dynamics but including BM motion and OHC charge coupling. We found similar qualitative behavior, which confirms that under our assumptions hair bundle motility is not important to produce compressive nonlinear behaviour. The stability analysis revealed that there is a large parameter region where the model does not require precise tuning of parameters.

The chief shortcoming of all the models we consider here is that they are purely local. In particular, they all ignore the process by which sound waves travel longitudinally along the BM. It is widely accepted that each longitudinal position codes for a particular input frequency, the so-called characteristic frequency (CF) of that location. The simplification inherent in all these models is that the nonlinear active process applies only to frequencies close to the particular CF frequency at the longitudinal position under consideration.

However, there is evidence to suggest that longitudinal coupling may indeed be present in the cochlea, and contribute significantly to the dynamics. The CF for a particular location

may be amplitude dependent, with the peak of the traveling wave shifting towards the base as input intensity is increased[2,5]. The fluid motion in and around the organ of Corti is not likely to be entirely planar, and may affect OHCs at nearby longitudinal positions[19]. The tectorial membrane is also capable of supporting longitudinal travelling waves[20]. In addition, it has been argued that a slight tilting of the OHC, so that the hair bundles are closer to the stapes than the base, can lead to a feed-forward amplification process[21]. It is perhaps unrealistic that the results of a local model could ever be closely matched to whole-organ experimental data; all such data will contain the influence of longitudinal coupling, and so a local model should not be expected to provide accurate quantitative comparison.

Several avenues of future work suggest themselves based on the results presented here. First, a more extensive investigation of the parameter space of the new model (10) would be useful, as would fitting its parameters to various physiological measurements, such as the properties of the Deiters' cells. Second, a more detailed understanding of the behavior of the ion channels is required in order to avoid the phenomenological choice of the form and argument of an open probability function[22]. Such a treatment might shed more light on the rate of compression, which in our models is close to saturation due to the Boltzmann open probability function P_{O}. It seems that the form of this nonlinearity rather than a cubic nonlinearity as is present in the normal-form models, or the presence of a local bifurcation is the key feature that gives a compressive nonlinear response that is observed in the BM motion as in Fig. 2. Finally, and most importantly, each of the models needs to be coupled to the longitudinal pressure-wave dynamics, in which a form of active mechanism is applied at each location along the basilar membrane. Until such a study is undertaken, the conclusions of this paper must be interpreted somewhat tentatively.

Acknowledgements

APPENDIX A: COMPRESSION RATE OF THE CUSP MODEL

A simple calculation can show that indeed equation (2) exhibits a $1/3$-power law in its large amplitude dynamic response. For example, using a harmonic balance method one can seek a solution as a truncated Fourier series $x(t) = a_0 + a_1 \cos \omega t + b_1 \sin \omega t$. Avoiding the symmetric case $\alpha = 0$ one can parametrize both the input amplitude and the vibration amplitude response $z = \sqrt{a_1^2 + b_1^2}$, by a_0, the DC part of the response; note that for $\alpha = 0$ such a parameterization is impossible. Specifically, we find

$$z^2(a_0) = \frac{2(\alpha + a_0\beta - a_0^3\sigma)}{3a_0} = \frac{2\alpha}{3\sigma a_0} + O(1) \tag{A1}$$

and

$$F^2(a_0) = \frac{(\beta a_0 - a_0^3\sigma + \alpha)\left((\alpha - a_0\beta + 5a_0^3\sigma)^2 + 4a_0^2\omega^2\right)}{6a_0^3\sigma} = \frac{\alpha^3}{6\sigma a_0^3} + O(a_0^{-2}) \tag{A2}$$

From these two asymptotic scalings, we see immediately a $1/3$-power law nonlinearity in the limit of large sound input, $F \to \infty$. In particular, note that $F \to \infty$ as $a_0 \to 0$. Hence $a_0 \to 0$ represents the limit of large sound input, and we have

$$\lim_{a_0 \to 0} \frac{\dfrac{\partial}{\partial a_0} \log z(a_0)}{\dfrac{\partial}{\partial a_0} \log F(a_0)} = \frac{1}{3}. \tag{A3}$$

APPENDIX B: DERIVATION OF THE OHC-DC-BM MODEL

We assume that the BM and HB are coupled through a simple mechanical system, where the HB has negligible mass. This coupling is described by the mechanical system

$$\begin{pmatrix} m_{bm}\ddot{x}_{bm} \\ 0 \end{pmatrix} + \begin{pmatrix} d_{bm} & d_{12} \\ d_{12} & d_{hb} \end{pmatrix} \begin{pmatrix} \dot{x}_{bm} \\ \dot{x}_{hb} \end{pmatrix} + \begin{pmatrix} k_{bm} & k_{12} \\ k_{12} & k_{hb} \end{pmatrix} \begin{pmatrix} x_{bm} \\ x_{hb} \end{pmatrix} = \begin{pmatrix} f_1 \sin \omega t - F_{dc} \\ f_2 \sin \omega t \end{pmatrix}. \tag{B1}$$

29

The right hand side of the equation corresponds to the forcing of the BM and HB from the Deiters' cell (DC) and the external forcing of the pressure difference between the two compartments of the cochlea. Note that k_{12} and d_{12} can be negative, but need to have the same sign. The OHC has its own stiffness and damping and can generate a force proportional to its charge

$$F_{\text{ohc}} = -k_{\text{ohc}}x_{\text{ohc}} - d_{\text{ohc}}\dot{x}_{\text{ohc}} - pq.$$

The DC is represented by a simple spring and damper. Assuming the reticular lamina does not move the DC length can be calculated from the constraints $x_{\text{dc}} = -x_{\text{bm}} - x_{\text{ohc}}$. Thus, the force excerted by the DC is

$$F_d = k_{\text{dc}}(x_{\text{bm}} + x_{\text{ohc}}) + d_{\text{dc}}(\dot{x}_{\text{bm}} + \dot{x}_{\text{ohc}}).$$

We assume that the OHC and DC damping and stiffnesses are proportional, that is, $d_{\text{ohc}}/k_{\text{ohc}} = d_{\text{dc}}/k_{\text{dc}}$. Solving $F_{\text{dc}} = F_{\text{ohc}}$ with this assumption we get

$$F_{\text{dc}} = \frac{k_{\text{ohc}}}{k_{\text{dc}} + k_{\text{ohc}}}(k_{\text{dc}}x_{\text{bm}} + d_{\text{dc}}\dot{x}_{\text{bm}}) - p\left(1 - \frac{k_{\text{ohc}}}{k_{\text{dc}} + k_{\text{ohc}}}\right)q.$$

From the equation of motion of the HB, we find that

$$d_{\text{hb}}\dot{x}_{\text{hb}} + k_{\text{hb}}x_{\text{hb}} = f_2 \sin \omega t - d_{12}\dot{x}_{\text{bm}} - k_{12}x_{\text{bm}}.$$

We want to replace $\dot{x}_{\text{hb}}$ in the first line of (B1), therefore we use

$$\begin{aligned}
d_{12}\dot{x}_{\text{hb}} + k_{12}x_{\text{hb}} &= \frac{d_{12}}{d_{hb}}\left(d_{\text{hb}}\dot{x}_{\text{hb}} + k_{\text{hb}}x_{\text{hb}} + \left(\frac{d_{\text{hb}}}{d_{12}}k_{12} - k_{\text{hb}}\right)x_{\text{hb}}\right) \\
&= \frac{d_{12}}{d_{hb}}\left(f_2 \sin \omega t - d_{12}\dot{x}_{\text{bm}} - k_{12}x_{\text{bm}} + \left(\frac{d_{\text{hb}}}{d_{12}}k_{12} - k_{\text{hb}}\right)x_{\text{hb}}\right).
\end{aligned}$$

to get

$$\ddot{x}_{\text{bm}} + 2\zeta\omega_0\dot{x}_{\text{bm}} + \omega_0^2\left(x_{\text{bm}} + f_{\text{hb}}x_{\text{hb}} - f_q q\right) = \nu_{\text{bm}}F \sin \omega t,$$

where

$$2\zeta\omega_0 = \frac{1}{m_{\text{bm}}}\left(d_{\text{bm}} - \frac{d_{12}^2}{d_{\text{hb}}} + \frac{d_{\text{dc}}k_{\text{ohc}}}{k_{\text{dc}} + k_{\text{ohc}}}\right),$$

$$\omega_0^2 = \frac{1}{m_{\text{bm}}}\left(k_{\text{bm}} - \frac{d_{12}k_{12}}{d_{\text{hb}}} + \frac{k_{\text{dc}}k_{\text{ohc}}}{k_{\text{dc}} + k_{\text{ohc}}}\right),$$

$$f_q = \frac{p}{m_{\text{bm}}\omega_0^2}\left(1 - \frac{k_{\text{ohc}}}{k_{\text{dc}} + k_{\text{ohc}}}\right),$$

$$f_{\text{hb}} = \left(m_{\text{bm}}\omega_0^2\right)^{-1}\left(k_{12} - \frac{d_{12}}{d_{\text{hb}}}k_{\text{hb}}\right),$$

$$\nu_{\text{bm}}F = \frac{1}{m_{\text{bm}}}\left(f_1 - \frac{d_{12}}{d_{\text{hb}}}f_2\right).$$

The hair bundle dynamics is described by

$$\dot{x}_{\text{hb}} = -\frac{k_{\text{hb}}}{d_{\text{hb}}}x_{\text{hb}} - \frac{d_{12}}{d_{\text{hb}}}\dot{x}_{\text{bm}} - \frac{k_{12}}{d_{\text{hb}}}x_{\text{bm}} + \frac{f_2}{d_{\text{hb}}}\sin\omega t.$$

If we assume that the hair bundle dynamics is fast, i.e., $\frac{k_{\text{hb}}}{d_{\text{hb}}} \gg 1$ then

$$x_{\text{hb}} = \frac{1}{k_{\text{hb}}}\left(f_2\sin\omega t - k_{12}x_{\text{bm}} - d_{12}\dot{x}_{\text{bm}}\right).$$

Putting this into the BM equation we get

$$\ddot{x}_{\text{bm}} + 2\zeta\omega_0\dot{x}_{\text{bm}} + \omega_0^2\left(x_{\text{bm}} - f_q q\right) = \nu_{\text{bm}}F\sin\omega t, \tag{B2}$$

where

$$2\zeta\omega_0 = \frac{1}{m_{\text{bm}}}\left(d_{\text{bm}} + \frac{d_{\text{dc}}k_{\text{ohc}}}{k_{\text{dc}} + k_{\text{ohc}}} - \frac{k_{12}d_{12}}{k_{\text{hb}}}\right),$$

$$\omega_0^2 = \frac{1}{m_{\text{bm}}}\left(k_{\text{bm}} + \frac{k_{\text{dc}}k_{\text{ohc}}}{k_{\text{dc}} + k_{\text{ohc}}} - \frac{k_{12}^2}{k_{\text{hb}}}\right),$$

$$f_q = \frac{p}{m_{\text{bm}}\omega_0^2}\left(1 - \frac{k_{\text{ohc}}}{k_{\text{dc}} + k_{\text{ohc}}}\right),$$

$$\nu_{\text{bm}}F = \frac{1}{m_{\text{bm}}}\left(f_1 - \frac{k_{12}}{k_{\text{hb}}}f_2\right).$$

Further, to account for the BM and HB sensitivity we define

$$\nu_{\text{hb}}F = \frac{f_2}{k_{\text{hb}}}, \ \gamma_{\text{bm}} = -\frac{k_{12}}{k_{\text{hb}}}, \ f_v = \frac{d_{12}}{k_{12}}.$$

The current adaptation is governed by the equation $\dot{x}_{\text{a}} = -\kappa(x_{\text{a}} - x_{\text{hb}})$ which becomes

$$\dot{x}_{\text{a}} = -\kappa\left\{x_{\text{a}} - \left(\gamma_{\text{bm}}x_{\text{bm}} + \gamma_{\text{bm}}f_v\dot{x}_{\text{bm}} + \nu_{\text{hb}}F\sin\omega t\right)\right\}. \tag{B3}$$

In case one wants to include the hair bundle dynamics, its equation with the new parameters becomes

$$\tau_{\mathrm{hb}}\dot{x}_{\mathrm{hb}} = -x_{\mathrm{hb}} + \gamma_{\mathrm{bm}}x_{\mathrm{bm}} + \gamma_{\mathrm{bm}}f_v\dot{x}_{\mathrm{bm}} + \nu_{\mathrm{hb}}F\sin\omega t, \qquad (\mathrm{B4})$$

where $\tau_{\mathrm{hb}} = d_{\mathrm{hb}}/k_{\mathrm{hb}}$.

REFERENCES

[1] A. J. Hudspeth, "Making an effort to listen: Mechanical amplification in the ear", Neuron **59**, 503–545 (2008).

[2] W. S. Rhode, "Basilar membrane mechanics in the 6-9kHz region of sensitive chinchilla cochleae", J. Acoust. Soc. Am. **121**, 2805–2818 (2007).

[3] H. Kennedy, A. Crawford, and R. Fettiplace, "Force generation by mammalian hair bundles supports a role in cochlear amplification", Nature **443**, 880–883 (2005).

[4] D. Ó Maoiléidigh and F. Jülicher, "The interplay between active hair bundle motility and electromotility in the cochlea", J. Acoust. Soc. Am. **128**, 1175–90 (2010).

[5] M. Ruggero, N. Rich, and L. Robles, "Basilar-membrane responses to tones at the base of the chinchilla cochlea", J. Acoust. Soc. Am. **101**, 2151–2163 (1997).

[6] V. M. Eguíluz, M. Ospeck, Y. Choe, A. J. Hudspeth, and M. O. Magnasco, "Essential nonlinearities in hearing", Phys. Rev. Lett. **84**, 5232–5235 (2003).

[7] Y. A. Kuznetsov, *Elements of Applied Bifurcation Theory* (Springer-Verlag, New York) (2004).

[8] T. Duke and F. Jülicher, "Active travelling wave in the cochlea", Phys. Rev. Lett. **90**, 158101 (2003).

[9] A. Kern and R. Stoop, "Essential role of couplings between hearing nonlinearities", Phys. Rev. Lett. **91** (2003).

[10] S. Camalet, T. Duke, F. Jülicher, and J. Prost, "Auditory sensitivity provided by self-tuned critical oscillations of hair cells", Proc. Natl. Acad. Sci. USA **97**, 3183–3188 (2000).

[11] R. Szalai, B. Epp, A. R. Champneys, and M. Homer, "On time-delayed and feed-forward transmission line models of the cochlea", J. Mech. Mat. Struct. **6**, 557–568 (2011), URL `http://msp.berkeley.edu/jomms/2011/6-1/p34.xhtml`.

[12] S. Elliot, E. Ku, and B. Linton, "Time domain model of a nonlinear inhomogeneous cochlear", in *Concepts and Challenges in the Biophysics of Hearing*, edited by N. Cooper and D. Kemp, 74–81 (World Scientific, 10th International Workshop on the Mechanics of Hearing, Keele 2008) (2009).

[13] E. Ku, S. Elliot, and B. Linton, "Periodicity of the spectrum of modelled spontaneous otoacoustic emmisions", in *Concepts and Challenges in the Biophysics of Hearing*, edited by N. Cooper and D. Kemp, 82–84 (World Scientific, 10th International Workshop on the Mechanics of Hearing, Keele 2008) (2009).

[14] G. Zweig and C. A. Shera, "The origin of periodicity in the spectrum of evoked otoacoustic emissions", J. Acoust. Soc. Am. **98**, 2018–2047 (1995).

[15] R. Szalai, *PDDE-CONT: A continuation and bifurcation software for delay-differential equations*, Department of Applied Mechanics, Budapest University of Technolgy and Economics (2005), available at `http://seis.bris.ac.uk/~rs1909/pdde/`.

[16] B. Nadrowski, P. Martin, and F. Jülicher, "Active hair-bundle motility harnesses noise to operate near an optimum of mechanosensitivity", Proc. Natl. Acad. Sci. U.S.A. **101**, 12195–12200 (2004).

[17] J. Tinevez, F. Jülicher, and P. Martin, "Unifying the various incarnations of active hair-bundle motility by the vertebrate hair cell", Biophys. J. **93**, 4053–4067 (2007).

[18] B. Lindner, K. Dierkes, and F. Jülicher, "Local exponents of nonlinear compression in periodically driven nonlinear oscillators", Phys. Rev. Lett. **103**, 250601 (2009).

[19] J. Meaud and K. Grosh, "The effect of tectorial membrane and basilar membrane longitudinal coupling in cochlear mechanics", J. Acoust. Soc. Am. **127**, 1411–1421 (2010).

[20] R. Ghaffari, A. J. Aranyosi, and D. M. Freeman, "Longitudinally propagating traveling waves of the mammalian tectorial membrane", Proc. Natl. Acad. Sci. U.S.A. **104**, 16510–16515 (2007).

[21] C. Steele and K. Lim, "Cochlear model with three-dimensional fluid, inner sulcus and feed-forward mechanism", Audiol. Neuro-Otol. **4**, 197–203 (1999).

[22] M. Beurg, J. Nam, A. Crawford, and R. Fettiplace, "The actions of calcium on hair bundle mechanics in mammalian cochlear hair cells", Biophys. J. **94**, 2639–2653 (2008).

TABLE I. Parameter values used in simulations of the Ó Maoiléidigh & Jülicher model (4).

Parameter	Value
D	60 nm
Δ	1.9305 nm^{-1}
δ	35.1951 nm
g	4×10^{-5} nA/μV
k_{gs}	8×10^{-3} N/m
γ	0.25
p	16 μV/nm
C_{ohc}	2×10^{-5} μF
λ	2×10^{-2} mNs/m
λ_{a}	2×10^{-2} mNs/m
μ_{hb}	1.05×10^{-3} mm^2
k	0.103 N/m
α_1	-6.91 nm/Pa
β_1	-8.12 mN
γ_1	0.530
I_{hb}	3nA
C_{eff}	$(C_{\text{ohc}}^{-1} + \beta_1 p^2)^{-1}$
F	20 μPa at 0 dB SPL

TABLE II. Parameter values used in simulations of the model (10).

Parameter	Value
ω_0	$6.6 \times 2\pi$ 1/ms
ζ	0.1
Δ	1.9305 nm^{-1}

ν_{bm}	3.1623×10^4 $(\text{mm})^3/\text{N}(\text{ms})^2$
ν_{hb}	9.4868 nm/Pa
κ	4.4 $1/\text{ms}$
γ	1.8 $1/\text{ms}$
γ_{bm}	10^{-3}
I_{hb}	3nA
f_q	$0 \text{ — } 1000$ mV/N
f_v	$0 \text{ — } 2$ $1/\text{ms}$
F	20 µPa at 0 dB SPL

LIST OF FIGURES

37